Opt Quant Electron (2016) 48:139
DOI 10.1007/s11082-015-0366-0

Comparisons of diffuse optical imaging between direct-current and amplitude-modulation instrumentations

Liang-Yu Chen[1,2] · Jhao-Ming Yu[1] · Min-Cheng Pan[3] · Sheng-Yih Sun[4] · Chia-Cheng Chou[4] · Min-Chun Pan[1,2]

Received: 28 August 2015 / Accepted: 29 December 2015 / Published online: 23 January 2016

Abstract Breast tissues like fatty and fibroglandular ones are adipose mainly and possess high scattering nature, so that they diffuse and make the light approximately uniformly distribute over the measured cross-section besides absorbing to reduce the light intensity. Strong cause-and-effect relationships exist between absorption and intensity decay, and between scattering and phase delay as well. Thereby in a diffuse optical imaging system it is a general practice to estimate absorption coefficients from the measured intensity since it reflects most of the absorption property. This study aims to illustrate that both μ_a and μ_s' images of breast can be reconstructed by only direct-current data reliably to a certain extent. Varied sets of phantom design with assigned absorption/scattering properties for inclusion and background were synthesized and image reconstructed to demonstrate this perspective. Moreover, we employed a slab-type diffuse optical imaging system with a dual-direction direct-current NIR measurement module, where reconstructed images were compared between with and without reflectance NIR data.

Keywords Diffuse optical imaging · Direct-current NIR · Amplitude-modulation NIR · Phantom design · Slab-type imaging module

This article is part of the Topical Collection on Micro/Nano Photonics for the International Year of Light 2015.

Guest Edited by Yen-Hsun Su, Lei Liu, Xinlong Xu and Zhenhua Ni.

✉ Min-Chun Pan
pan_minc@cc.ncu.edu.tw

[1] Department of Mechanical Engineering, National Central University, Taoyuan City 320, Taiwan, R.O.C.

[2] Graduate Institute of Biomedical Engineering, National Central University, Taoyuan City 320, Taiwan, R.O.C.

[3] Department of Electronic Engineering, Tung-Nan University, New Taipei City 222, Taiwan, R.O.C.

[4] Tao-Yuan General Hospital, Taoyuan City 330, Taiwan, R.O.C.

1 Introduction

The common used noninvasive biomedical imaging modalities for the screening and diagnosis of breast tumor, such as sonography and X-ray mammography, can illustrate structural information of breast tissue. Besides mammography involving the issue of ionizing radiation, those imaging modalities are still trapped in overlapped structures that result in false diagnosis. Therefore, although still in clinical validation, some other alternatives using non-ionizing radiation techniques such as optical (visible or invisible) (Gibson and Dehghani 2009) and microwave (Semenov 2009) ones have been considered and implemented for the diagnosis of breast tumor in the past decades. Among those, diffuse optical imaging (DOI) is an emerging technique that can provide physiological and pathological information about the breast. Both the absorption- and scattering-property distribution of the breast can be obtained through near infrared DOI (NIR DOI). Furthermore, oxyhemoglobin, deoxyhemoglobin, water, and lipid concentrations in the breast can be evaluated if the various spectra information is available (Corlu et al. 2005; Srinivasan et al. 2005). Following the phantom experiments and verification, clinical trials usually have to be carried out to assess the potential of the developed DOI system.

The DOI plays an important role as an approach to monitor oxy-haemoglobin and deoxy-haemoglobin concentrations, which reflect both physiological and pathological conditions of tissue. In terms of instrumentation design the DOI systems have been developed mainly in three types including continuous-wave (CW) modes such as direct-current (DC) (Iftimia and Jiang 2000; Pei et al. 2001; Xu et al. 2002; Pan et al. 2009), amplitude-modulation (AM) (mostly called frequency-domain, FD) (Srinivasan et al. 2005; Zhang et al. 2005; Fang et al. 2009), and pulse-wave mode (frequently called time-domain, TD) (Enfield et al. 2007). Some literature and monographs (Arridge and Lionheart 1998; Harrach 2009; Jiang 2011) addressed the issue of their differences. For the instrumentation of FD modes, the phase (or time) delay data, not available from a DC one, can be further acquired. However, the introduction of accompanied FD devices usually increases the cost and draws extra measurement issue such as system saturation due to expansion of the dynamic range of NIR illumination. Therefore, it is nontrivial to investigate the credibility of using DC measurement to reconstruct optical-property images especially when the DOI images are used for tumor screening instead of diagnosis.

In this paper, three synthesized phantoms all associated with an inclusion with designated optical properties were analyzed to address the crosstalk issue between absorption and scattering properties. The results demonstrate that the reconstructed μ_a and $\mu_s^{'}$ images using DC data are still able to convey functional information about tissue for the differentiation between tumor and background even if reconstructed images using AM data are less influenced by crosstalk effects. Based on the promising results obtained from synthesized case study, a slab-type DOI system with acquiring dual-directional NIR DC transmission data was implemented and employed for the reconstruction of μ_a and $\mu_s^{'}$ images in a practical way. Further, in addition to transmission data, reflection NIR data was also acquired to soothe artifacts in reconstructed images in this study.

2 Methods

2.1 Image reconstruction basis

The image reconstruction of DOI contains solving both the forward and the inverse problems. For the former, the diffusion equation, Eq. (1), expressed in the frequency domain is utilized as a forward model to describe the physical process of the light diffused in a highly scattering medium (Paulsen and Jiang 1995; Schweiger et al. 2005; Dehghani et al. 2009)

$$\nabla \cdot D(\mathbf{r})\nabla\Phi(\mathbf{r},\omega) - \left[\mu_a(\mathbf{r}) - \frac{i\omega}{c}\right]\Phi(\mathbf{r},\omega) = -S(\mathbf{r},\omega), \tag{1}$$

where $\Phi(\mathbf{r},\omega)$ is the photon density at position $\mathbf{r}$; ω is the light modulation frequency; $S(\mathbf{r},\omega)$ is the isotropic source term; c is the speed of light in tissue; and μ_a and D denote the optical absorption and diffusion coefficients, respectively. Moreover, the diffusion coefficient is dependent upon the reduced scattering coefficient μ_s', as $D = 1/[3(\mu_a + \mu_s')]$. As $\omega = 0$, Eq. (1) further becomes to the process in a direct-current format for illuminated light source. For solving this forward model, numerical computation based on the finite element method (FEM) with a boundary condition, $-D\nabla\Phi \cdot \hat{n} = \alpha\Phi$, can be implemented, where $\hat{n}$ is the unit normal vector for the boundary surface, α is the coefficient related to the internal reflection at the boundary.

In solving the inverse problem, the inverse solution to estimate the optical-property distribution is obtained by a numerical way with iteratively minimizing the differences between the measured diffusion photon density data Φ^M around the tissue and the computational model data Φ^C from solving the forward problem by the FEM with the current estimated optical properties. This data-model misfit difference is defined as

$$\chi^2 = \sum_{i=1}^{N_M} \left[\Phi_i^C - \Phi_i^M\right]^2, \tag{2}$$

where N_M is the number of measurement data. However, minimizing this defined data-model misfit difference usually runs into difficulty with an ill-conditioned problem, which usually happens in DOI image reconstruction. Therefore, the use of regularization techniques is needed to remedy the problem. To tackle both the ill-posed and ill-condition problems of computing Eq. (2), various studies targeted to develop effective regularization schemes (Pogue et al. 1999; Li et al. 2003; Cao et al. 2007; Douiri et al. 2007; Hiltunen et al. 2009; Chen et al. 2012, 2013). In this work, the constrained estimate of $\Delta\mu$ can be obtained by using Tikhonov regularization and solved the following equation

$$\left(\mathbf{J}^T\mathbf{J} + \lambda\mathbf{I}\right)\Delta\mu = \mathbf{J}^T\Delta\Phi, \tag{3}$$

where $\Delta\mu$ is the update vector composed of $\Delta\mu_a$ and ΔD, the update length from current estimated optical properties, $\mathbf{J} = \left[\partial\Phi^C/\partial\mu_a \quad \partial\Phi^C/\partial D\right]$ is the Jacobin matrix, λ is the regularization parameter, and $\Delta\Phi$ is the vector of data-model misfit at each measurement location. Besides, as the Jacobian matrix involves derivatives with respect to absorption and diffusion coefficients, in Eq. (3) it is normalized by a diagonal matrix G consisting of the current estimate of the optical properties to diminish absorption–scattering cross-talk effect during reconstruction (Dehghani et al. 2009), i.e., $\tilde{\mathbf{J}} = \mathbf{JG}$, where $\mathbf{G} = diag([\mu_a; D])$.

Figure 1 shows the flowchart of the optical-property image reconstruction algorithm. Based on the flowchart, a MATLAB-coded image reconstruction program, named as NIR·FD_PC (Pan et al. 2008, Pan and Pan 2010; Chen et al. 2012, 2013), was developed. The adjoint method (Arridge and Schweiger 1995) was used to efficiently evaluate Eq. (3) in this reconstruction program. Besides, varied regularization schemes such as Tikhonov regularization that has been widely used in DOI image reconstruction, and edge-preserving regularization were implemented in this image reconstruction program. It should be noted

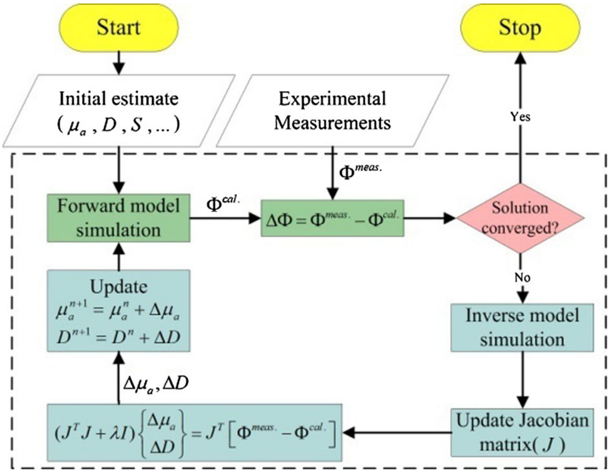

Fig. 1 Flowchart of optical-property image reconstruction algorithm

that for the same comparison basis Tikhonov regularization and the normalized Jacobian matrix as described above were adopted for the following reconstruction results to address the absorption–scattering cross-talk issue when reconstructing images from DC and FD data respectively.

2.2 Slab-type DOI system

A stand-along slab-type DOI system was built up to complete and reconstruct optical mammograms; further, the NIR scanning module associated with compression plates can be integrated with a commercialized X-ray mammography unit to compose dual imaging modalities (Yu et al. 2013). This module collects both bidirection transmissive and reflective NIR data for optical-property image reconstruction; and the design of the scanning module is using two translation slabs moving on the compression plates for the reconstruction of a bulk image if necessary, otherwise a slice (μ_a or μ_s') image is computed. In contrast to the work of Massachusetts General Hospital (Zhang et al. 2005; Fang et al. 2009), it employed a fixed source-detection configuration with down to top NIR illumination.

Figure 2 depicts the block diagram of our slab-type DOI system with a DC measurement module for compressed phantoms or tissue. The cranio–caudal view was adopted for the design. Currently the system employs a 5-mW laser module (LDCU5/8202, Power Technology) with a wavelength of 830 nm, of which the NIR light feeds into an optical switch (FOSW-1-16-N-62-L-2, Enaco) with a 1-by-16 optical fiber bundle. The 17 fibers of the bundle are pure silica core (62.5 µm) with silicone clad, suitable for transmission wavelengths from 700 to 900 nm, and each fiber has a diameter of 1.2 mm. The source light is delivered through the central one fiber in the bundle, and 14 of the remaining fibers surrounding it are delivered to the source ends with collimators (10 mm in diameter) on the top and bottom slabs made of aluminum alloy (AL6061). Each of the ends makes contact with the optical plate. The fiber bundle is 1 m in length and extends from the instrument cart to the phantom/tissue interface. The efficiency of the optical switching is approximately 83 %, yielding an average source power of 4 mW at the phantom/tissue surface.

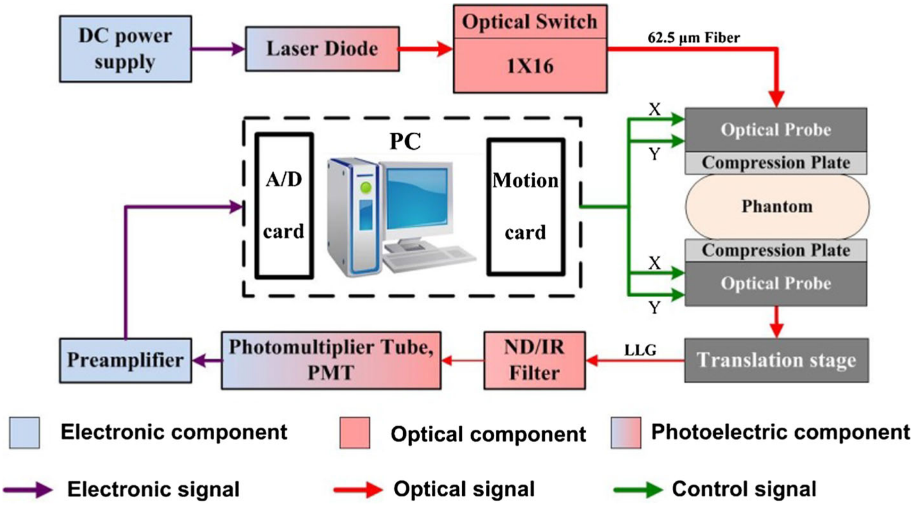

Fig. 2 Block diagram of the diffuse optical imaging system for compressed phantoms or tissues. The dual-direction optical probe mounted on two XY translation tables include pair-arranged source fibers and detection liquid light guides

For each source excitation, light transmission is recorded by seven surface locations on the opposite slab. For both slabs, out-emitted NIR is transmitted to 14 liquid light guides (LLG, 77635, Newport, USA) in series, which are mounted on a translation stage (AL6061). All LLG channels are detected by a single photomultiplier tube (PMT 7732-10, Hamamatsu) moving to the corresponding LLG to collect its out-emitted NIR. It is noted that a neutral density filter (ND filter, OD 0.6–4, LAMBDA) and an IR filter (830 ± 1 nm, 830FS10-12.5, Andover corp.) are mounted prior to the PMT, and used to attenuate received NIR intensity so that the dynamic range of PMT is able to accommodate the reduced light. The PMT is driven by a dedicated power supply (C7169, Hamamatsu) to obtain a gain control. A fixed gain (1.7×10^7) is set and used for the PMT module through the power supply generating a voltage of 1.1 V to its control line, which causes the PMT in a high voltage condition. Such a PMT can reliably measure optical power in a range of 0.2–12 nwatt. Then, the detected NIR current is pre-amplified and transferred into voltage with a gain of 80 mV/μA; further, the analogue voltage is digitized and acquired by a data acquisition card (NI PCI6122, National Instruments) associated with a pre-programmed LabVIEW®-coded man/machine interface for each detection in series. Besides, this multipurpose DAQ card is used to switch NIR light source, and drive the ND filter as well as stepping motors to move two scanning slabs and the translation stage.

3 Results and discussion

In this section, the comparison of the reconstruction images using DC and FD data respectively through simulation are presented to address the absorption–scattering cross-talk issue. More specifically, the computed absorption distribution of inclusion deviates from its original assignment the same as that of background phantom, which arises from the cross talk between absorption and scattering properties. Likewise, the computed scattering distribution deviating from its designation, which arises from absorption characteristics, is also illustrated. In the simulation, the synthetic phantoms were designed with using a homogeneous background of 80-mm diameter and an embedded 15-mm-diameter inclusion (or tumor) of different optical contrast levels, where the inclusion is put 20 mm off the center of background. The test phantoms were assigned optical properties using $\mu_s^{'} = 1.0\ \text{mm}^{-1}$ and $\mu_a = 0.01\ \text{mm}^{-1}$ for background, which are reconciled with the finding (Spinelli et al. 2004) that $\mu_s^{'}$ and μ_a are ranging between (0.9, 1.6 mm^{-1}) and (0.003, 0.012 mm^{-1}) respectively, to generate simulation data for image reconstruction. The simulation data were obtained from the forward solution of the finite-element diffusion model with designed optical properties in place. Specifically, the modulation frequency of excitation NIR was using 100 MHz for FD data, and a total of 256 amplitude and 256 phase-delay data points were generated by 16 measurement locations for each of 16 light source positions. Moreover, randomly generated noise of 1 % in amplitude (both DC and FD data) and 1° deviation in phase delay (FD data) were added into the simulation data. For all the reconstructions, 30 iterations were used during the reconstruction procedure and the stopping criterion, $\left\|\Phi^{n-1} - \Phi^{n}\right\|^2 \Big/ \|\Phi^{n}\|^2 < 10^{-3}$, was met.

Based on the experimental finding that the tumor-background optical contrast was around 2 (Jiang et al. 2002), the following three trials with varied contrasts of the optical properties were examined to investigate and address the absorption–scattering cross-talk issue:

- Case (1): the inclusion relative to the background with a contrast of 2 for both μ_a and $\mu_s^{'}$;
- Case (2): the inclusion relative to the background with a contrast of 2 for only μ_a, and the same $\mu_s^{'}$ as the background;
- Case (3): the inclusion relative to the background with a contrast of 2 for only $\mu_s^{'}$, and the same μ_a as the background.

For case (1), Fig. 3 shows the reconstruction results using DC (Fig. 3a, c) and FD data (Fig. 3b, d), in the designated phantom the embedded inclusion relative to the background medium was assigned a contrast of 2 for both μ_a and $\mu_s^{'}$. As can be seen, the characteristics of reconstructed μ_a and $\mu_s^{'}$ images show excellent quality regardless of using DC or FD data in this test case. For case (2), Fig. 4 presents the reconstructed images computed with μ_a of the inclusion relative to background with a contrast of 2. Apparently, Fig. 4a, c using DC data for image reconstruction demonstrate a considerable cross-talk phenomenon, i.e., the observed scattering variations in the reconstructed image arise from the difference in absorption properties. Moreover, even reconstruction using FD data, it is noted that the cross-talk phenomena still exist in the images as shown in Fig. 4b, d, but it reduces from $\mu_s^{'} = 1.4348\ \text{mm}^{-1}$ using DC data to $\mu_s^{'} = 1.3358\ \text{mm}^{-1}$. In the case of (3), Fig. 5 illustrates the reconstructed images using $\mu_s^{'}$ of the inclusion relative to background with a contrast of 2. Similar to case (2) shown in Fig. 4, with using DC data the computed absorption distribution (Fig. 5a, c) deviating from the original assignment arises from the cross-talk and contribution of scattering properties. It is shown in Fig. 5b, d that as using FD data in case (3) the cross-talk effect for μ_a can be reduced from 0.0154 to 0.0131 mm^{-1}. Therefore, from Figs. 4 and 5 it can be observed that using FD data the cross-talk effect cannot be removed completely, but the unwanted situation can be soothed. Although the DC NIR data acquisition supplies no phase delay information, it is noted from the above results that the reconstructed μ_a and $\mu_s^{'}$ images still enable to differentiate the variation of tissue. As the absorption and scattering properties of tissue indicate

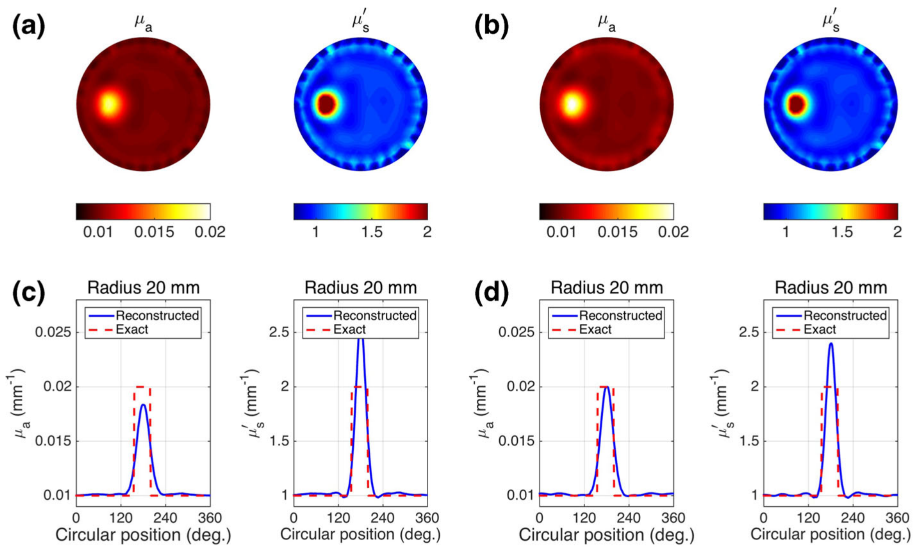

Fig. 3 Simulated reconstructions of μ_a and $\mu_s^{'}$ images for an inclusion relative to background with a contrast of 2 for both μ_a and $\mu_s^{'}$. **a**, **b** Reconstructed μ_a and $\mu_s^{'}$ images through using the DC and FD data, respectively, **c**, **d** one-dimensional (1D) circular profiles cutting through the images of **a** and **b**

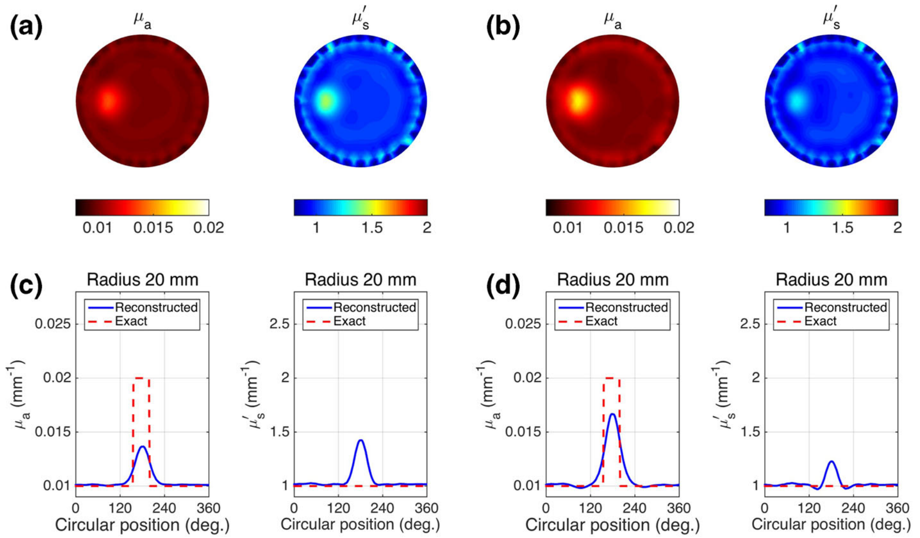

Fig. 4 Simulated reconstructions of both μ_a and $\mu_s^{'}$ images for the inclusion with a contrast of 2 for μ_a (μ_s' of inclusion and background the same). **a**, **b** Reconstructed μ_a and μ_s' images through using the DC and FD data, respectively, **c**, **d** 1D circular profiles cutting through the images of **a** and **b**

functional difference, therefore, the DOI images with using DC data may reflect functional difference for tissue screening. This implies that a DC imaging system it is still appropriate for the screening of breast tumor.

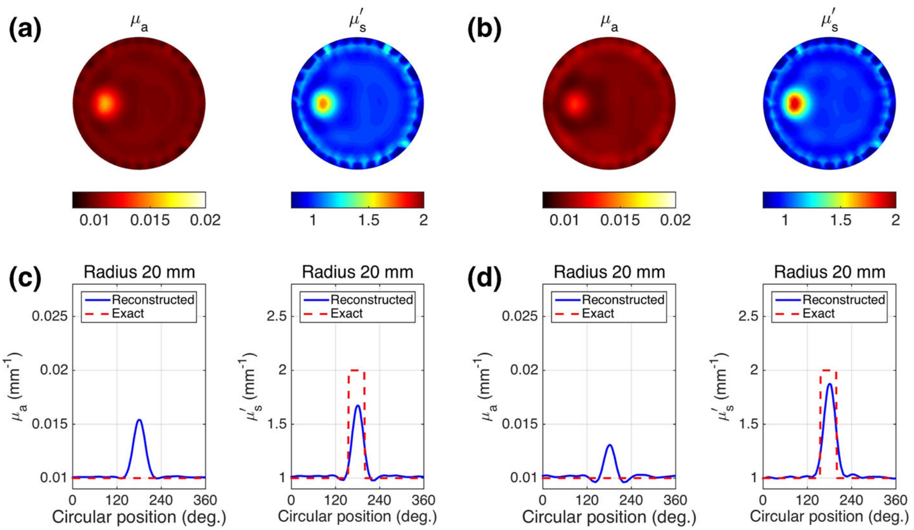

Fig. 5 Simulated reconstructions of both μ_a and μ_s' images for the inclusion with a contrast of 2 for μ_s' (μ_a of inclusion and background the same). **a**, **b** Reconstructed μ_a and μ_s' images through using the DC and FD data, respectively, **c**, **d** 1D circular profiles cutting through the images of **a** and **b**

It is noted that μ_a and μ_s' images can both be reconstructed with using DC data for breast images. Although a prominent theoretical study (Arridge and Lionheart 1998) demonstrated that there exist the same steady-state (or direct-current) boundary data under the conditions of different distributed optical properties, and suggested that simultaneous *unique* recovery of reduced scattering and absorption coefficients cannot be achieved when only DC data are employed, several experimental studies (Iftimia and Jiang 2000; Pei et al. 2001; Xu et al. 2002) still succeeded in the reconstruction of these two optical-property coefficients. In these experimental works, reconstruction algorithm incorporating regularization and/or the precondition technique that normalizing and scaling the Jacobian matrix were used to simultaneous recover the optical coefficients and to reduce the cross-talk effect. Analogous to these works, the results presented here were also reconstructed by the similar approach, i.e., using the algorithms incorporating regularization and the normalized Jacobian matrix. Otherwise, without this approach, the cross-talk issue would be even worse. Therefore, the explanation for this deemed conflict between theoretical study and experimental works is actually the fact that in the experimentation the reconstruction algorithms incorporate regularization and precondition techniques to handle the ill-posed inverse problem in DOI (Xu et al. 2002; Harrach 2009).

As shown in Fig. 6, a breast-like phantom embedded with a shallow and a deep inclusion (10 and 40 mm from the top of phantom, respectively) on the slab-type DOI system was conducted measurement for image reconstruction. The geometrical dimension of breast-like phantom with optical properties of $\mu_s' = 0.6\ \text{mm}^{-1}$ and $\mu_a = 0.006\ \text{mm}^{-1}$ is a combination of a half sphere (diameter 100 mm) and a cylinder (length 40 mm). The inclusion possesses an optical contrast of 4 with respect to the phantom background. Here dual-direction DC NIR data were collected for computation. Figure 7 shows the reconstructed optical-property images, where (a) and (b) are absorption and scattering images with a shallow inclusion, (c) and (d) are absorption and scattering images with a deep inclusion; furthermore, for each figure (a), (b), (c) or (d) the left is obtained using

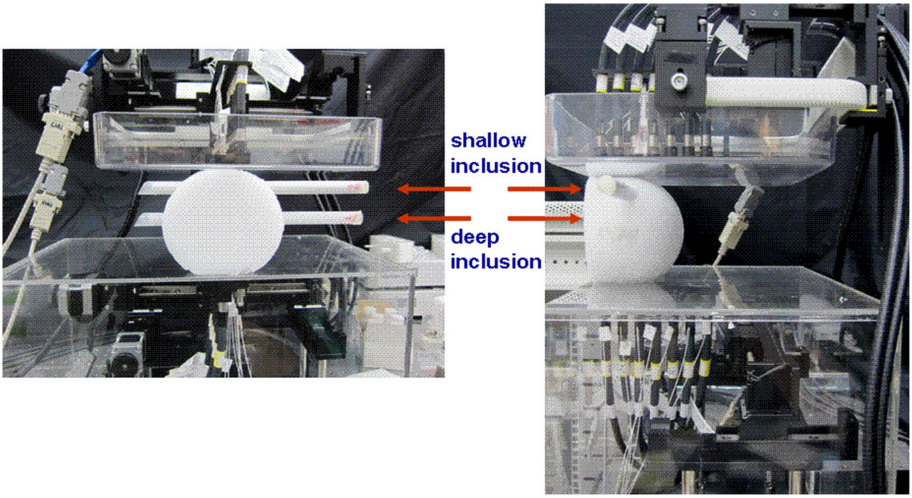

Fig. 6 Illustration of breast-like phantom embedded with shallow and deep inclusions, 10 and 40 mm from top respectively, on the slab-type DOI system with dual-directional NIR acquisition for image reconstruction

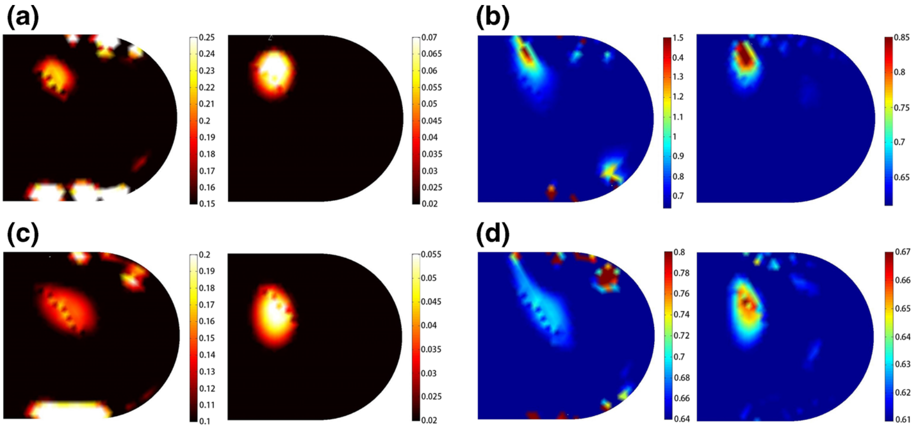

Fig. 7 Reconstructed DOI images. **a** Absorption images and **b** scattering images with a shallow inclusion, **c** absorption images and **d** scattering images with a deep inclusion, where the *left* using transmission NIR data and the *right* using both transmission and reflectance data for each figure (**a**), (**b**), (**c**) or (**d**)

transmission NIR data, and the right is computed using both transmission and reflectance data. It is noted that μ_a and $\mu_s^{'}$ images can be reconstructed through using DC data, and if both the transmission and reflectance data are applied, the inclusion can be characterized better with less artifacts.

4 Conclusions

In this paper, we presented the results of the reconstructed μ_a and $\mu_s^{'}$ images using both the DC and FD NIR data to address the issue of crosstalk effect on image reconstruction. Then, a slab-type DOI imaging system with a DC measurement module was employed to reconstruct μ_a and $\mu_s^{'}$ images of a breast like phantom. The reconstruction results show that the absorption and scattering images using DC data can still be evaluated to a certain extent with the use of penalty term and/or priori information during the computation of regularization. Therefore, because μ_a images reflect functional information in tissue and the simplicity of constructing DC instrumentation, it is anticipated that to operate a DC imaging system at multi-wavelength illumination is appealing and least expensive for breast screening although the system operated in the FD can acquire additional phase information to identify lesions more accurately.

Acknowledgments We would like to acknowledge funding from the Ministry of Science and Technology in Taiwan through Grants 101-2221-E-008-010-MY2, 101-2221-E-008-093-MY3, and 101-2221-E-236-014.

References

Arridge, S.R., Lionheart, W.R.B.: Nonuniqueness in diffusion-based optical tomography. Opt. Lett. **23**, 882–884 (1998)

Arridge, S.R., Schweiger, M.: Photon-measurement density functions. Part 2: finite-element-method calculations. Appl. Opt. **34**, 8026–8037 (1995)

Cao, N., Nehorai, A., Jacob, M.: Image reconstruction for diffuse optical tomography using sparsity regularization expectation–maximization algorithm. Opt. Express **15**, 13695–13708 (2007)

Chen, L.-Y., Pan, M.-C., Pan, M.-C.: Implementation of edge-preserving regularization for frequency-domain diffuse optical tomography. Appl. Opt. **51**, 43–54 (2012)

Chen, L.-Y., Pan, M.-C., Pan, M.-C.: Flexible near-infrared diffuse optical tomography with varied weighting functions of edge-preserving regularization. Appl. Opt. **52**, 1173–1182 (2013)

Corlu, A., Choe, R., Durduran, T., Lee, K., Schweiger, M., Arridge, S.R., Hillman, E.M.C., Yodh, A.G.: Diffuse optical tomography with spectral constraints and wavelength optimization. Appl. Opt. **44**, 2082–2093 (2005)

Dehghani, H., Srinivasan, S., Pogue, B.W., Gibson, A.: Numerical modelling and image reconstruction in diffuse optical tomography. Philos. Trans. R. Soc. A **367**, 3073–3093 (2009)

Douiri, A., Schweiger, M., Riley, J., Arridge, S.R.: Anisotropic diffusion regularization methods for diffuse optical tomography using edge prior information. Meas. Sci. Technol. **18**, 87–95 (2007)

Enfield, L.C., Gibson, A.P., Everdell, N.L., Delpy, D.T., Schweiger, M., Arridge, S.R., Richardson, C., Keshtgar, M., Douek, M., Hebden, J.C.: Three-dimensional time-resolved optical mammography of the uncompressed breast. Appl. Opt. **46**, 3628–3638 (2007)

Fang, Q., Carp, S.A., Selb, J., Boverman, G., Zhang, Q., Kopans, D.B., Moore, R.H., Miller, E.L., Brooks, D.H., Boas, D.A.: Combined optical imaging and mammography of the healthy breast: optical contrast derived from breast structure and compression. IEEE Trans. Med. Imaging **28**, 30–42 (2009)

Gibson, A., Dehghani, H.: Diffuse optical imaging. Philos. Trans. R. Soc. A **367**, 3055–3072 (2009)

Harrach, B.: On uniqueness in diffuse optical tomography. Inverse Probl. **25**, 055010 (2009)

Hiltunen, P., Prince, S.J.D., Arridge, S.: A combined reconstruction-classification method for diffuse optical tomography. Phys. Med. Biol. **54**, 6457–6476 (2009)

Iftimia, N., Jiang, H.: Quantitative optical image reconstruction of turbid media by use of direct-current measurements. Appl. Opt. **39**, 5256–5261 (2000)

Jiang, H.: Diffuse Optical Tomography—Principles and Applications. CRC Press, Boca Raton (2011)

Jiang, H., Iftimia, N.V., Xu, Y., Eggert, J.A., Fajardo, L.L., Klove, K.L.: Near-infrared optical imaging of the breast with model-based reconstruction. Acad. Radiol. **9**, 186–194 (2002)

Li, A., Miller, E.L., Kilmer, M.E., Brukilacchio, T.J., Chaves, T., Stott, J., Zhang, Q., Wu, T., Chorlton, M., Moore, R.H., Kopans, D.B., Boas, D.A.: Tomographic optical breast imaging guided by three-dimensional mammography. Appl. Opt. **42**, 5181–5190 (2003)

Pan, M.-C., Pan, M.-C.: Rapid convergence on the inverse solution regularized with the Lorentzian distributed function for near infrared continuous wave diffuse optical tomography. J. Biomed. Opt. **15**, 016014 (2010)

Pan, M.-C., Chen, C.-H., Chen, L.-Y., Pan, M.-C., Shyr, Y.-M.: Highly resolved diffuse tomography: a systematic approach using high-pass filtering for value-preserved images. J. Biomed. Opt. **13**, 024022 (2008)

Pan, M.-C., Chen, C.-H., Pan, M.-C., Shyr, Y.-M.: Near infrared tomographic system based on high angular resolution mechanism—design, calibration, and performance. Measurement **42**, 377–389 (2009)

Paulsen, K.D., Jiang, H.: Spatially varying optical property reconstruction using a finite element diffusion equation approximation. Med. Phys. **22**, 691–701 (1995)

Pei, Y., Graber, H.L., Barbour, R.L.: Normalized-constraint algorithm for minimizing inter-parameter crosstalk in DC optical tomography. Opt. Express **9**, 97–109 (2001)

Pogue, B.W., McBride, T.O., Prewitt, J., Osterberg, U.L., Paulsen, K.D.: Spatially variant regularization improves diffuse optical tomography. Appl. Opt. **38**, 2950–2961 (1999)

Schweiger, M., Arridge, S.R., Nissila, I.: Gauss–Newton method for image reconstruction in diffuse optical tomography. Phys. Med. Biol. **50**, 2365–2386 (2005)

Semenov, S.: Microwave tomography: review of the progress towards clinical applications. Philos. Trans. R. Soc. A **367**, 3021–3042 (2009)

Spinelli, L., Torricelli, A., Pefferi, A., Taroni, P., Danesini, G.M., Cubeddu, R.: Bulk optical properties and tissue components in the female breast from multiwavelength time-resolved optical mammography. J. Biomed. Opt. **9**, 1137–1142 (2004)

Srinivasan, S., Pogue, B.W., Jiang, S., Dehghani, H., Paulsen, K.D.: Spectrally constrained chromophore and scattering NIR tomography provides quantitative and robust reconstruction. Appl. Opt. **44**, 1858–1869 (2005)

Xu, Y., Gu, X., Khan, T., Jiang, H.: Absorption and scattering images of heterogeneous scattering media can be simultaneously reconstructed by use of dc data. Appl. Opt. **41**, 5427–5437 (2002)

Yu, J.-M., Chen, L.-Y., Chiang, H.-C., Pan, M.-C., Sun, S.-Y., Chou, C.-C., Pan, M.-C.: Parallel scanning architecture for mammogram-based diffuse optical imaging. ASME Trans. J. Med. Devices **7**(2), 020936 (2013)

Zhang, Q., Brukilacchio, T.J., Li, A., Stott, J.J., Chaves, T., Hillman, E., Wu, T., Chorlton, M., Rafferty, E., Moore, R.H., Kopans, D.B., Boas, D.A.: Coregistered tomographic X-ray and optical breast imaging: initial results. J. Biomed. Opt. **10**, 024033 (2005)